QoS-driven optimized design-based integrated visible light communication and positioning for indoor IoT networks

Yang, Helin; Zhong, Wen-De; Chen, Chen; Alphones, Arokiaswami; Du, Pengfei

2019

Yang, H., Zhong, W.-D., Chen, C., Alphones, A., & Du, P. (2020). QoS-driven optimized design-based integrated visible light communication and positioning for indoor IoT networks. IEEE Internet of Things Journal, 7(1), 269-283. doi:10.1109/JIOT.2019.2951396

https://hdl.handle.net/10356/142888

https://doi.org/10.1109/JIOT.2019.2951396

QoS-Driven Optimized Design-Based Integrated Visible Light Communication and Positioning for Indoor IoT Networks

Helin Yang, *Student Member, IEEE*, Wen-De Zhong, *Senior Member, IEEE*, Chen Chen, *Member, IEEE*, Arokiaswami Alphones, *Senior Member, IEEE*, and Pengfei Du

***Abstract*—With the rapid development of the Internet of Things (IoT) in the smart city, smart grid, and smart industry, indoor communication and positioning are important for IoT. However, radio-frequency (RF)-based wireless networks may fail to guarantee different quality-of-service (QoS) requirements of devices, due to the limited bandwidth, severe interference, and multipath reflections. Hence, this article presents a new integrated visible light communication (VLC) and VLC positioning (VLCP) network for IoT to provide both high-speed communication and high-accuracy positioning services. As the network consists of multiple VLC access points (APs), we propose jointly optimizing the AP selection, bandwidth allocation, adaptive modulation, and power allocation approach to satisfy different QoS requirements of indoor devices while maximizing the network data rate. A low-complexity iterative algorithm is presented to solve the resource management (RM) optimization problem by decomposing it into two subproblems. Finally, a robust handover mechanism and a pedestrian dead reckoning (PDR)-assisted VLCP scheme are presented to maintain good performance under line-of-sight (LOS) blockages. The simulation results verify that the proposed solutions outperform other existing solutions in terms of effectively enhancing the data rate, improving the positioning accuracy, and guaranteeing devices' QoS requirements. In detail, the mean position error is reduced from 20 to 4.3 cm by using our presented integrated VLCP model. The proposed RM approach achieves a satisfied QoS level improvement of up to 20.3% compared with the non-QoS-driven RM approach, and it achieves the high data rate up to 1.31 Gb/s.**

***Index Terms*—Internet of Things (IoT), link blockage, quality of service (QoS), resource management (RM), robust scheme, visible light communication (VLC) and VLC positioning (VLCP).**

Manuscript received October 9, 2019; revised October 27, 2019; accepted October 31, 2019. Date of publication November 5, 2019; date of current version January 10, 2020. This work was supported in part by the National Natural Science Foundation of China under Grant 61901065, in part by the Delta-NTU Corporate Laboratory for Cyber-Physical Systems with funding support from Delta Electronics, Inc., and in part by the National Research Foundation Singapore through the Corp Lab@University. *(Corresponding author: Chen Chen.)*

H. Yang, W.-D. Zhong, and A. Alphones are with the School of Electrical and Electronic Engineering, Nanyang Technological University, Singapore 639798 (e-mail: hyang013@e.ntu.edu.sg).

C. Chen is with the School of Microelectronics and Communication Engineering, Chongqing University, Chongqing 400044, China (e-mail: c.chen@cqu.edu.cn).

P. Du is with the Singapore Institute of Manufacturing Technology (SIMTech), Agency for Science, Technology and Research (A*STAR), Singapore 138634.

Digital Object Identifier 10.1109/JIOT.2019.2951396

I. Introduction

With the various application services of devices (e.g., mobile phones, monitors, and sensors) in wireless networks, Internet of Things (IoT) has been emerging as a promising vision for next generation networks through realizing smart manufacturing, smart grid, and smart city [1], [2]. *Note:* Acronyms of full forms are shown in Table I.

However, several challenges need to be considered for IoT when operating the wireless communication techniques in radio-frequency (RF)-based wireless networks. First, it is difficult for the RF-based wireless networks to support the huge connectivity and guarantee different quality-of-service (QoS) requirements of IoT devices due to the limited bandwidths in the RF band [1], [3], [4]. Second, the severe electromagnetic interference may lead to the financial loss for industries, or even the physical damage for human safety [5]. Last but not least, the indoor RF-based localization systems [such as wireless-fidelity (Wi-Fi), Bluetooth, ultra wideband (UWB), etc.] are still inaccurate and unreliable in the IoT networks due to the multipath reflections and shadowing [3], [6], [7]–[10].

Recently, visible light communication (VLC) and visible light positioning (VLP) have been identified as promising candidates to provide high-speed-data transmission and high-accuracy positioning in indoor environments [3], [4], [7], where about 80% of wireless data usage is by indoor devices [11]. Many studies [12]–[16] have adopted VLC for indoor IoT networks to offer high data rate and guarantee different QoS requirements of IoT devices. In [12], a VLC-based IoT architecture was presented for indoor and outdoor deployments. Liu *et al.* [13] and Shao *et al.* [14] proposed the light energy harvesting models to support communication services, where the energy from light signals is harvested by IoT devices over VLC downlink and the harvested energy is used for the data transmissions over RF links. Moreover, the hybrid VLC/RF IoT networks were presented to offer the better service to devices [15], [16], where the VLC network can support the high data rate and the RF network guarantees the seamless coverage.

On the other hand, VLP has become an attractive research topic recently due to its high positioning accuracy compared with the RF-based localization systems [7], [17]–[25]. Some VLP system models were presented to support indoor localization, tracking, and navigation services for IoT

TABLE I
ACRONYMS OF FULL FORMS

Acronym	Full form	Acronym	Full form
IoT	Internet of Things	APs	Access Points
RF	Radio Frequency	LOS	Line Of Sight
VLC	Visible Light Communication	VLP	Visible Light Positioning
QoS	Quality of Service	SG	Subcarrier Group
LEDs	Light Emitting Diodes	OOBI	Out-Of-Band Interference
RSS	Received Signal Strength	ICI	Inter-Cell Interference
PD	Photo-Detector	RSSI	RSS Indicator
PDR	Pedestrian Dead Reckoning	FBMC	Filter Bank Multicarrier
SCM	Subcarrier Multiplexing	QAM	Quadrature Amplitude Modulation
OFDMA	Orthogonal Frequency Division Multiple Access	SINR	Signal-to-Interference-plus-Noise-Ratio
RSE	Root Square Error		

devices [20]–[25]. Shao *et al.* [23] and Zhuang *et al.* [24] experimentally evaluated the real-time localization schemes using the received signal strength (RSS) algorithm for IoT devices with high positioning accuracy. In [20] and [21], the novel imaging processing frameworks-based high-precision VLP systems were investigated in indoor rooms, but they need highly complicated image sensor arrays at receivers. Moreover, Ma *et al.* [25] presented a new indoor localization technique based on VLP that allows IoT devices to obtain high positioning accuracy with low signal processing complexity and power consumption.

As a matter of fact, most of the studies only focused on VLC [11]–[16] or VLP independently [19]–[25] in the indoor IoT networks, where both communication and positioning services might be expected at the same time for IoT devices in practical indoor environments (e.g., offices, hospitals, supermarkets, factories, etc.). So far, several works [17], [18], [26], [27] presented their integrated VLC and VLP systems (called VLCP) to provide both communication and positioning purposes. For example, the combination of orthogonal frequency-division multiple access (OFDMA) and RSS algorithm was presented in [17] and [18], but high out-of-band interference (OOBI) generated from signals may degrade the positioning performance. Moreover, the filter bank multicarrier-based subcarrier multiplexing (FBMC-SCM)-assisted-VLP with the high signal processing complexity was proposed to reduce the OOBI [26], [27]. However, the works [17], [18], [26], [27] only considered a single cell, where indoor environments consist of multiple VLC access points (APs) and intercell interference (ICI) greatly degrades the system performance [28]–[33].

It is worth noting that both high-speed data rate and high positioning accuracy strongly depend on the line-of-sight (LOS) link in VLC and VLP systems, while the LoS link is often partially or completely blocked due to the mobility of devices and human beings in practical indoor environments [34]. In this case, the network performance is notably affected and the satisfied QoS levels are decreased. To the best of our knowledge, almost all of the above works [7]–[33] did not investigate how to satisfy minimum data rate requirements of devices and maintain high positioning accuracy performance under blockages in the dynamic IoT networks.

According to the above discussion, some fundamental questions arise: Will the integrated VLC and VLP systems be able to provide both the high-speed communication and high-accuracy positioning services for devices? How do we maintain both the communication and positioning performance when LOS blockages happen in the dynamic integrated VLCP IoT networks? Will the resource management (RM) strategy be capable of guaranteeing the requirement of both the minimum data rate and the positioning accuracy of the IoT devices? Moreover, the performance of the integrated system is degraded due to the high OOBI generated from OFDM signals on adjacent subcarriers. In addition, ICI and LOS blockages significantly degrade the network performance.

Motivated by the above observations and in order to solve the problem, in this article, we first present a new integrated VLCP network to achieve both communication and positioning purposes for indoor IoT devices. Then, a joint AP section, subcarrier group (SG) allocation, adaptive modulation, and power allocation approach is proposed to maximize the network data rate while guaranteeing the QoS requirements (i.e., the minimum data rate and the positioning accuracy) of IoT devices. The LOS blockage issue is investigated in the IoT networks, and the robust optimized schemes are presented to maintain the network performance. The main contributions of this article are summarized as follows.

1) For the first time, in this article, in order to achieve both the communication and positioning purposes for indoor IoT devices, we present a new integrated VLCP IoT network, where the RSS sinusoidal positioning signals can be put into the idle frequency holes to avoid OOBI on the positioning frequencies.
2) We investigate the optimization problem of joint AP section, SG allocation, adaptive modulation, and power allocation in multicell integrated VLCP IoT networks under different QoS requirements of devices. We solve the optimization problem with low complexity.
3) We propose robust schemes to reduce the negative effect of the LOS blockage on the network performance in the dynamic integrated VLCP IoT networks. Specifically, we propose a robust handover mechanism to maintain a high data rate. In addition, a robust positioning scheme is proposed to guarantee high positioning accuracy by combining PDR [35] with the RSS-based VLP model under LOS blockages.

The rest of this article is organized as follows. The new integrated VLCP IoT network model is presented in Section II. Section III formulates the optimization problem and the solution is provided in Section IV. Section V shows the robust schemes under LoS blockages. The extended applications of the presented work for IoT are provided in Section VI. The simulation results and analysis are offered in Section VII. Finally, Section VIII concludes this article.

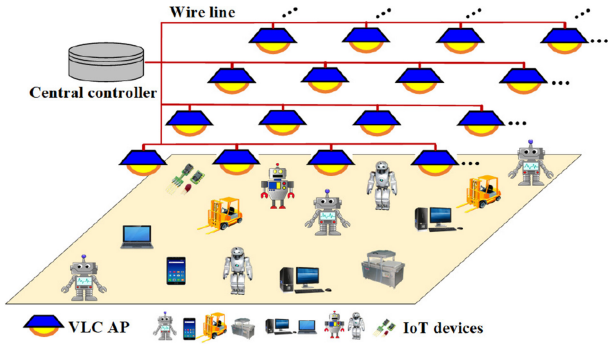

Fig. 1. Indoor integrated VLCP network for IoT devices.

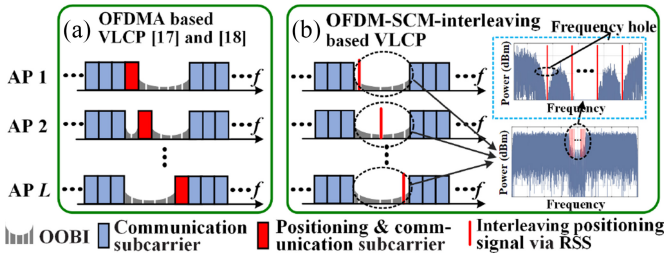

Fig. 2. Spectrum structures of the integrated VLCP IoT network.

II. Integrated VLCP System Model

We consider an indoor IoT application scenario based on the integrated VLCP networks, which consists of a set of L VLC APs uniformly installed on the ceiling and each VLC AP covers a confined area to generate a small optical cell, as shown in Fig. 1. In addition to offer the lighting requirements, the network also provides both the communication and positioning services for indoor IoT devices. In the network, the communication and positioning signals are modulated into the APs before passing through the wireless optical channel, and each IoT device is equipped with a photo-detector (PD) to convert the received light into electrical signals.

In the IoT network, a number of IoT devices (K devices) are randomly located in the lighting coverage area, and some IoT devices may suffer from ICI from adjacent cells when they are in the overlapped areas. There exists a central controller in the network, which connects all APs to broadcast information to IoT devices, and the uplink feedback is offered by the Wi-Fi links. After receiving the feedback information, the central controller can tackle the RM task. All available subcarriers are equally divided into $N+1$ SGs, where the subcarriers in the $(N+1)$th SG are used for positioning and the remaining N SGs are served for communication. In order to improve the subcarrier utilization, the network adopts the unity frequency reuse (UFR) design in the integrated VLCP IoT network, where the communication SGs are reused across all cells. Let $\mathcal{L}$ and $\mathcal{K}$ denote the AP set and the IoT device set, respectively. Let $\mathcal{N}_l$ denote the SG set in the lth cell.

In this section, we describe the existing and proposed integrated VLCP models, the communication model, and the RSS-based positioning model.

A. New Integrated VLCP Model

1) OFDMA-Based VLCP via RSS [17], [18]: The scheme directly combines the OFDM modulation and 2-D RSS positioning algorithm for the integrated VLCP system, as shown in Fig. 2(a), where the L identified subcarriers are used for positioning. The positioning subcarriers are also used for communication. Here, each positioning subcarrier with respect to its corresponding AP is used for indoor positioning. The detailed procedures to implement OFDMA-based VLCP via RSS can be seen in [17] and [18]. However, as shown in Fig. 2(a), the OFDM signals usually leak relatively high OOBI to subcarriers, which degrades both the communication and positioning performance of the integrated VLCP system.

2) Proposed OFDM-SCM-Interleaving-Based VLCP via RSS: As shown in Fig. 2(b), we can observe that there exist several specific frequencies (called frequency holes) having the negligible OOBI from the OFDM signal when these subcarriers are not used to transmit the OFDM signal (idle subcarriers). In this case, the sinusoidal positioning signals (red color) can be put into the frequency holes, which can avoid the OOBI on the positioning frequencies from the adjacent communication subcarriers and hence achieve higher positioning accuracy performance as compared with the OFDMA-based VLCP. In addition, the RSS indicator (RSSI) at each IoT device can be adopted for the AP selection in the multicell networks, which will be analyzed in the next section.

At each AP, the sinusoidal signals for VLP are added with the OFDM signal after allocating the SGs to devices, where the L positioning subcarriers from f_1 to f_L are all in the $(N+1)$th SG and the communication data for the devices are all on the N SGs. After collecting the feedback information [channel information, signal-to-interference-plus-noise-ratio (SINR), QoS requirements, RSSI, etc.,] from the IoT devices, the communication data stream is then encoded to the OFDM signal with the adaptive quadrature amplitude modulation (QAM) mapping based on the devices' minimum data rate requirements and the received SINR values.

At the device, on the one hand, the RSSI values on the positioning subcarriers from different APs can be measured by devices, and the locations of devices can be estimated by using the RSS-based positioning algorithm, which will be shown in Section II-C. On the other hand, the communication signal can be obtained when the received signal passes through the band-stop filter (BSF), and the OFDM demodulation method is applied to demodulate the communication signal.

B. Communication Model

For the optical link, the LOS channel gain between the lth AP and the kth device is expressed as

$$G_{k,l} = \frac{(m_l+1)A_r}{2\pi d_{k,l}^2}\cos^{m_l}(\phi_{k,l})T_s(\psi_{k,l})g(\psi_{k,l})\cos\psi_{k,l} \quad (1)$$

where A_r denotes the PD's active area. $d_{k,l}$, $\phi_{k,l}$, and $\psi_{k,l}$ are the distance, the angle of irradiance, and the angle of incidence between the lth AP and the kth device, respectively. m_l denotes the order of Lambertian emission of the lth AP. $T_s(\psi_{k,l})$ and $g(\psi_{k,l})$ are the gains of the optical filter and the

optical concentrator, respectively. The channel gain depends on the characteristics of LEDs and PDs as well as the transmission distance.

At the receiver, the received SINR at the kth device if it assigns on the nth SG of the lth AP is given by

$$\gamma_{k,n,l}^{\mathrm{co}} = \frac{\mu^2 P_{n,l}\left(G_{k,n,l}\right)^2}{\sum_{i=1,i\neq l}^{L} P_{n,i}\left(G_{k,n,i}\right)^2 + \delta^2} \tag{2}$$

where μ is the PD's responsivity. $P_{n,l}$ is the allocated electrical power on the nth SG at the lth AP. $G_{k,n,l}$ represents the optical channel gain from the lth AP to device k on the nth SG. $\sum_{i=1,i\neq l}^{L} P_{n,i}(G_{k,n,i})^2$ denotes ICI from other cells. δ^2 is the noise power, including the shot noise (denoted by δ_{shot}^2), the thermal noise (denoted by $\delta_{\mathrm{thermal}}^2$), and the intersymbol interference (ISI, denoted by δ_{ISI}^2) caused by the multipath propagation [3], [6], which can be expressed as

$$\delta^2 = \delta_{\mathrm{shot}}^2 + \delta_{\mathrm{thermal}}^2 + \delta_{\mathrm{ISI}}^2. \tag{3}$$

In (3), the received signals at the PD through diffuse path may suffer from multipath propagation which causes ISI in complex indoor environments. The more details about the above-mentioned multipath propagation can be found in [3] and [6].

At the kth device, if it assigns the nth SG of the lth AP and the OFDM signal is modulated by $M_{k,n,l}$-QAM with the modulation order $M_{k,n,l}$, the bit error rate (BER) can be approximated by using [36]

$$\mathrm{BER}_{k,n,l} = \frac{\sqrt{M_{k,n,l}} - 1}{\sqrt{M_{k,n,l}}\log_2\left(\sqrt{M_{k,n,l}}\right)} erfc\left(\sqrt{\frac{3\gamma_{k,n,l}^{\mathrm{co}}}{2\left(M_{k,n,l}-1\right)}}\right). \tag{4}$$

The available data rate (bps) of the kth device across allocated SGs at the lth AP can be expressed as [36]

$$R_k = B_n \sum_{n=1}^{N} \rho_{k,n,l}\log_2 M_{k,n,l} \tag{5}$$

where B_n is the bandwidth of the nth SG. $\rho_{k,n,l}$ is a binary variable, $\rho_{k,n,l} \in \{0, 1\}$, and $\rho_{k,n,l} = 1$ indicates the nth communication SG is allocated to the k-device at the lth AP; otherwise, it takes the value 0.

C. RSS-Based Positioning Model

For the kth device, the received electrical power (also called RSSI) on the lth positioning subcarrier from the lth AP can be expressed as $P_{k,l}^{\mathrm{rec}} = G_{k,l}P_l$ [17]–[19]. In addition, assuming the PD axis and the AP axis are perpendicular to the ceiling, we have $\cos(\phi_{k,l}) = \cos(\psi_{k,l}) = h/d_{k,l}$ with h being the height from APs to the receiver plane [17]–[19]. Consequently, $G_{k,l}$ in (1) can be rewritten as

$$G_{k,l} = \frac{h^{m_l+1}(m_l+1)A_r}{2\pi d_{k,l}^{m_l+3}} T_s\left(\psi_{k,l}\right) g\left(\psi_{k,l}\right) = C(m_l+1)\frac{h^{m_l+1}}{d_{k,l}^{m_l+3}} \tag{6}$$

where $C = A_r T_s(\psi_{k,l}) g(\psi_{k,l})/2\pi$ is a constant value which depends on the characteristics of LEDs and PDs. Then, the received electrical power $P_{k,l}^{\mathrm{rec}}$ is rewritten as

$$P_{k,l}^{\mathrm{rec}} = P_{i,l}C(m_l+1)h^{m_l+1}/d_{k,l}^{m_l+3}. \tag{7}$$

From (7), we can derive the distance $d_{k,l}$ as follows:

$$d_{k,l} = \sqrt[m_l+3]{P_{i,l}C(m_l+1)h^{m_l+1}/P_{k,l}^{\mathrm{rec}}}. \tag{8}$$

Let $\mathbf{\Theta}_k = (x_k, y_k)$ and $\mathbf{\Theta}_l = (x_l^{\mathrm{led}}, (x_l^{\mathrm{led}})$ denote the locations of the kth device and the lth AP, respectively. The device coordinates $\mathbf{\Theta}_k$ correspond to the APs coordinates $\mathbf{\Theta}_l$ based on the following group of equations:

$$\left(x_k - x_l^{\mathrm{led}}\right)^2 + \left(y_k - y_l^{\mathrm{led}}\right)^2 = d_{k,l}^2 - h^2, \qquad l \in \mathcal{L}. \tag{9}$$

When the received power $P_{k,l}^{\mathrm{rec}}$ is measured at the kth device, the distance $d_{k,l}$ can be calculated by (8). Finally, the estimated location of the device can be calculated by using the RSS-based trilateration algorithm [17]–[19], the detailed procedures to implement the 2-D RSS-based positioning can be seen in [17] and [18]. Let $\mathbf{\Theta}_k^{\mathrm{e}} = (x_{k,\mathrm{e}}, y_{k,\mathrm{e}})$ denote the estimated location of the kth device. The positioning error [root square error (RSE)] of the kth device is given by

$$\mathrm{RSE}_k = \sqrt{\left(x_{k,\mathrm{e}} - x_k\right)^2 + \left(y_{k,\mathrm{e}} - y_k\right)^2}. \tag{10}$$

III. QoS Requirements and Problem Formulation

A. QoS Requirements in Integrated VLCP IoT Networks

In the IoT networks, some certain QoS requirements of devices should be considered in the optimized design, which will be discussed and analyzed as follows.

1) Minimum Data Rate Requirements of VLC: The minimum data rate requirements of some devices may range from low data rates to high data rates, which should be satisfied in the performance optimization design. Thus, the resulting constraint is expressed by

$$R_k \geq R_k^{\min} \tag{11}$$

where $R_k^{\min}$ is the minimum data rate threshold of the kth device.

2) Positioning Accuracy Requirements of VLP: In addition to the requirement in (11), the IoT network should guarantee the positioning accuracy requirement of the devices that need positioning services.

Without loss of generality, when other parameters are fixed, the RSE can be expressed as an explicit function of transmit electrical powers by using the Cramer–Rao lower bound (CRLB) [37]. Then, the CRLB on the RSE of the kth device is given by [37]

$$\mathrm{RSE}_k^{\mathrm{CRLB}} \geq \sqrt{\mathrm{tr}\left(\mathbf{J}^{-1}\left(\Theta_k^{\mathrm{e}}, \boldsymbol{P}_{\mathrm{po}}\right)\right)} \tag{12}$$

where $\mathbf{J}(\cdot)$ is the Fisher information matrix (FIM) and $\boldsymbol{P}_{\mathrm{po}}$ is the transmit electrical power vector on the positioning subcarriers at the selected APs with the selected corresponding highest RSSI. Due to space limitations, see [37] for all the analysis processes. Hence, we have the constraint

$$\sqrt{\mathrm{tr}\left(\mathbf{J}^{-1}\left(\Theta_k^{\mathrm{e}}, \boldsymbol{P}_{\mathrm{po}}\right)\right)} \leq \mathrm{RSE}_k^{\max} \tag{13}$$

where $\mathrm{RSE}_k^{\max}$ is the tolerant positioning error threshold of the kth device.

B. Problem Formulation

In the IoT network, our objective is to maximize the overall network transmission data rate while guaranteeing the above-mentioned QoS requirements of devices shown in Section III-A. Here, the RM problem (joint AP selection, SG allocation, adaptive modulation, and power allocation) can be mathematically formulated as

$$\begin{aligned}
&\max_{\boldsymbol{\alpha},\boldsymbol{\rho},\boldsymbol{M},\boldsymbol{P}} R_{\text{sum}} = \sum_{l\in\mathcal{L}}\sum_{k\in\mathcal{K}} \alpha_{k,l} R_k \\
&\text{s.t.} \quad \text{a: (11), (13)} \\
&\text{b: } \alpha_{k,l},\ \rho_{k,n,l} \in \{0,1\} \quad \forall k \quad \forall l \quad \forall n \\
&\text{c: } \sum_{l\in\mathcal{L}} \alpha_{k,l} = 1 \quad \forall k \\
&\text{d: } \sum_{k\in\mathcal{K}}\sum_{n\in\mathcal{N}_l} \rho_{k,n,l} P_{n,l} \le P_{\max} \quad \forall l \\
&\text{e: } \sum_{k\in\mathcal{K}}\sum_{n\in\mathcal{N}_l} \rho_{k,n,l} \le N \quad \forall l
\end{aligned} \tag{14}$$

where $\boldsymbol{\alpha}$, $\boldsymbol{\rho}$, $\boldsymbol{M}$, and $\mathbf{P}$ represent the matrix or vectors of the AP selection, SG allocation indicator, modulation order, and transmit power level, respectively. In order to reduce the AP selection complexity, constraint "c" in (14) is used to ensure that one device can only select a single AP to apply the communication services. Constraint "d" in (14) is that the transmit power of each AP allocated to its served devices should not exceed the maximum transmit power. Constraint "e" in (14) is imposed to guarantee that the sum of assembled SGs should not exceed the number of the available SGs of each AP.

IV. Solution to the Resource Management

Clearly, the optimization problem in (14) is a mixed-integer programming problem because the binary variables and the non-negative power variables are involved, as well as it is nonconvex, so it cannot be solved directly. Hence, we should make the optimization problem tractable. In this section, we solve the joint optimization problem in (14) by decomposing it into two subproblems: 1) AP selection with SG allocation and 2) adaptive modulation and power allocation. Consequently, after solving these two subproblems alternately, we can achieve the optimized solution of the joint optimization problem in (14) by using an iterative algorithm.

A. AP Selection Formation

The IoT network generally consists of multiple optical cells, hence the VLC AP selection should be considered to improve the network performance and guarantee IoT devices' QoS requirements. The traditional max-RSSI approach [38] is widely adopted to address the AP selection problem, but it fails to enable devices to achieve the desired service qualities because the devices may simply associate with the nearest AP with the largest RSSI value, which may result in intense channel contention and significant unbalanced data rate distributions. In addition, some optimal AP selection approaches [28]–[33] were theoretically presented in the RF networks or VLC networks, but they have the high complexity and the perfect assumption of devices' location information.

Hence, we propose a new AP selection approach to find the suitable AP selection strategy in the VLCP IoT network, where the strategy has the following functions: 1) VLP APs could satisfy the different QoS requirements of devices and 2) the AP selection needs to optimize the overall network performance. In short, the objective of the AP selection is to balance data rate distributions in the whole network, minimize the overall ICI, satisfy minimum data rate requirements of devices, and optimize the network data rate, which will be realized by the following analysis.

Considering the fact that different IoT devices have different service requirements, we first divide the devices into two kinds of devices based on their different services.

1) *Primary Devices:* Devices in this group have specific requirements on low service delay, high transmission reliability, and service steadiness, such as instant online software installation and real-time data streaming.
2) *Secondary Devices:* This kind of devices are not interested in the service delay and steadiness, such as short message service, web browsing, software/document downloading, and e-mail sending.

We set that primary devices have the higher priority to associate its needed AP, while second devices are with the lower priority to associate its needed AP compared with the primary devices. Let $\mathcal{K}_{\text{AP},l}$ denote the set of devices currently selected by the lth AP.

Implementation: Now, we show how to implement VLC AP selection step by step.

Step 1 (Candidate AP Selection): Each device first sorts the RSSI values of all APs in the candidate-selected AP subset, and it searches its nearest AP (the highest RSSI) denoted by AP_k, which refers to the candidate-selected AP, hence we have

$$\text{AP}_{(k)} = \arg\ \max_{l\in\mathcal{L}} \left(P_{k,l}^{\text{rec}}\right). \tag{15}$$

If more than one device select the same candidate AP and the corresponding AP has no device association, the AP selects the primary devices to associate its channel resource with the high priority. Other secondary devices should search their next nearest APs if this candidate AP has no enough channel and power resource for them, until each device searches its unique candidate AP. If more than one device with the same priority level select the same candidate AP, the AP adopts the proportional fair (PF)-priority scheduling scheme to serve the devices from the high PF-priority device to the low PF-priority device if the AP has enough resource [39]; otherwise, the low PF-priority devices have to select their next nearby APs.

Hence, according to the above analysis, each AP $l \in \mathcal{L}$ has its current candidate-served device set, which is expressed as

$$\mathcal{K}_{\text{AP},l} = \left\{ \text{AP}_{(k)}^{*} : k \in \mathcal{K} \right\}. \tag{16}$$

After completing the AP selection strategy, the minimum data requirements and service quality can be effectively guaranteed. However, the network still needs to adjust the candidate AP selection strategy to address the following issues.

1) Balance the data rate distributions, where some APs may be idle while other APs are busy serving devices,

leading to the unbalanced resource allocation. Hence, the networks need to adjust its AP selection strategy to optimize the overall network performance, which is shown in step 2.

2) Minimize the overall ICI to improve the network performance, which is shown in step 3.

Step 2 (Resource Balance-Based-AP Selection Adjustment): For the idle APs, the candidate-served device set of the l'th idle AP is expanded first by including the nearby devices with a certain range d_0, which is written as

$$\mathcal{K}_{\mathrm{AP},l'} = \left(\mathcal{K}_{\mathrm{AP},l'} \cup \left\{k \in \mathcal{K}_{\mathrm{AP},l} : \sqrt{(x_l - x_k)^2 + (y_l - y_k)^2} \le d_0\right\}\right). \tag{17}$$

In (17), the l'th idle AP selects the kth device from the lth AP candidate-served device set: $\mathcal{K}_{\mathrm{AP},l} = \mathcal{K}_{\mathrm{AP},l} - \{k\}$, but the update subset $\mathcal{K}_{\mathrm{AP},l} \neq \emptyset$. If the kth device was included in several idle APs, it would select the nearest idle AP.

Step 3 (ICI Minimum-Based-AP Selection Adjustment): We would like to mention that the device locating in the overlapping area may suffer severe ICI form adjacent cells, leading to the significant degradation of the network performance and the satisfied QoS level. However, if the device changes its decision by selecting the nearby AP with the lower ICI instead of its current associated AP, its performance and satisfied QoS level can be effectively improved. Based on this observation, the network needs to adjust the AP selection strategy to reduce the negative effect of ICI on the network performance improvement. Here, we define the signal-to-interference ratio (SIR) as the RSSI value of the current associated AP over the sum of the RSSI values from other adjacent APs (or optical cells). When the kth device currently associates with the lth AP, its SIR can be written as

$$\mathrm{SIR}_{k,l} = P_{k,l}^{\mathrm{rec}} \Bigg/ \left(\sum_{\hat{l} \in \mathcal{L},\, \hat{l} \neq l} P_{k,\hat{l}}^{\mathrm{rec}}\right). \tag{18}$$

Similarly, according to the RSSI values, the device can calculate other SIR values if it selects other APs, and it compares its current $\mathrm{SIR}_{k,l}$ with $\mathrm{SIR}_{k,\hat{l}}$, $\hat{l} \in \mathcal{L}$, and finally, selects the AP from the these candidate APs with the highest SIR value by

$$\mathrm{AP}_{(k)} = \arg \max_{l \in \mathcal{L}} \left(\mathrm{SIR}_{k,l}\right). \tag{19}$$

B. Suboptimal SG Allocation

We can observe that the optimization problem in (14) is a combinatorial problem, which has a prohibitive computational complexity if we solve it through using the exhaustive search for all the possible cases, especially, when the number of devices and SGs is large in the network. Hence, we propose a low complexity scheme to achieve the suboptimal SG allocation under the constraints in (11). The goal of the SG allocation is to flexibly allocate subcarrier resource of each cell to meet devices' minimum data rate requirement as well as maximize the overall network data rate.

The key principle of the proposed approach is that the primary devices first access the SGs of its selected AP, and the primary device whose rate is the farthest away from its target minimum data rate requirement has the priority to be allocated the SGs with highest channel quality to meet its minimum data rate requirement. Then, the AP allocates the excess SG resource to the secondary devices to meet their minimum data rate requirement. After satisfying the devices' QoS requirements, we allocate the excess SGs of each AP to the devices with high channel gains to maximize the overall network data rate.

Let Ω_k denote the SG subset allocated to the kth device. The proposed AP selection and SG allocation approach is shown in Algorithm 1.

Algorithm 1 AP Selection and SG Allocation

Initialize: $\mathcal{N}_l = \{1, \ldots, N\}$, $\mathcal{K} = \{1, \ldots, K\}$, set $R_k = 0$ and $\Omega_k = \emptyset$ for $\forall k \in \mathcal{K}$.

Step 1: AP selection

The AP selection strategy is carried out by the candidate AP selection, resource balance and ICI minimum based-AP selection adjustment shown by Section IV-A.

Step 2: Satisfy minimum rate requirements

Primary devices access SGs of its selected AP with the higher priority while secondary devices are with the lower priority to access SGs. The devices with the same priority level take step 3 to step 5.

For any device k satisfying $R_k < R_k^{\min}$;

Find the device k' satisfying $R_{k,\min} - R_k \le R_{k',\min} - R_{k'}$ for $\forall k' \in \mathcal{K}$;

For the device k', find SG $n' \in \mathcal{N}_l$ from its selected AP l with the highest data rate;

Let $\Omega_{k'} = \Omega_{k'} \cup \{n'\}$, $\mathcal{N}_l = \mathcal{N}_l - \{n'\}$, and update $R_{k'}$;

Step 3: Allocate excess SGs to maximize the sum data rate

If $\mathcal{N}_l \neq \emptyset$, $\forall l$, allocate the excess SGs to the devices with high channel gains to maximize the sum data rate.

C. Joint Adaptive Modulation and Power Allocation

Given the AP selection and SG allocation strategy, in each cell, the joint adaptive modulation and power allocation are presented to improve the network performance and guarantee the QoS requirements shown in (11) and (13). The details to implement it are shown in the following analysis.

When the BER target is $\mathrm{BER}_{\max}$, the modulation thresholds can be expressed as [34]

$$\begin{aligned} \gamma_j^{\mathrm{th}} &= \left(\gamma_{k,n,l}^{\mathrm{co}}\right)_{M_{k,n,l}} \\ &= \frac{3\left(M_{k,n,l} - 1\right)}{2} erfc^{-1}\left(\mathrm{BER}_{\max} \frac{\sqrt{M_{k,n,l}} \log_2\left(\sqrt{M_{k,n,l}}\right)}{\sqrt{M_{k,n,l}} - 1}\right) \\ M_{k,n,l} &= 2^j,\ j = 1, \ldots, J \end{aligned} \tag{20}$$

where $erfc^{-1}(\cdot)$ is the inverse $erfc$-function, and $\gamma_1^{\mathrm{th}} \le \gamma_2^{\mathrm{th}} \le \cdots \le \gamma_J^{\mathrm{th}}$. Then, the network can select the modulation order according to the SINR value $\gamma_{k,n,l}^{\mathrm{co}}$, which is

$$M_{k,n,l} = \begin{cases} 0, & \gamma_{k,n,l}^{\mathrm{co}} < \gamma_1^{\mathrm{th}} \\ 2^j, & \gamma_j^{\mathrm{th}} \le \gamma_{k,n,l}^{\mathrm{co}} \le \gamma_{j+1}^{\mathrm{th}}, \qquad j = 1, \ldots, J-1 \\ 2^J, & \gamma_J^{\mathrm{th}} \le \gamma_{k,n,l}^{\mathrm{co}}. \end{cases} \tag{21}$$

The above analysis in (20) and (21) presents the selection of the modulation order according to the feedback SINR values from devices. The adaptive modulation scheme can effectively

improve the transmission data rate and guarantee the devices' minimum data rate requirements.

Due to the severe attenuation of LEDs in the high-frequency domains in the VLC systems, the power allocation is applied to compensate for the frequency attenuation at APs. Considering the conventional power allocation scheme is not optimal due to the attenuation of high-frequency domains is balanced at the cost of the SINR reduction of low frequency domains, Wang *et al.* [40] presented a weighted power allocation design to improve the communication performance of all sub-bands. However, power allocation in [40] was still not the efficient approach in terms of the network throughput improvement due to the only fixed-order modulation format. Moreover, the power allocation variables on the positioning subcarriers should be carefully set to satisfy the positioning accuracy requirements, and the interference leakage from the two adjacent communication SGs to the positioning SG should not be too large to generate the high OOBI on the positioning SG, which directly degrades the positioning performance. Hence, the adaptive modulation and power allocation should be adaptively updated to optimize the network capacity while guaranteeing the QoS requirements of the IoT devices.

For the kth device in the lth cell, the nth SG signal in the frequency domain with the joint adaptive modulation and power allocation can be given by

$$\begin{aligned} &\boldsymbol{S}'_k\big(M_{k,n,l}, P_{n,l}, \rho_{k,n,l}\big) \\ &= P_{n,l} \cdot \boldsymbol{H}_k^{-1}\big(\rho_{k,n,l}\big) \cdot \boldsymbol{S}_k\big(M_{k,n,l}, P_{n,l}, \rho_{k,n,l}\big) \end{aligned} \tag{22}$$

where $\boldsymbol{S}'_k(M_{k,n,l}, P_{n,l}, \rho_{k,n,l})$ and $\boldsymbol{S}_k(M_{k,n,l}, P_{n,l}, \rho_{k,n,l})$ are the nth SG signal vectors in the frequency domain before and after power allocation and pre-equalization, respectively. $\boldsymbol{H}_n$ is the transfer pre-equalization matrix of the nth SG' subcarriers, and $\boldsymbol{H}_n$ is also a diagonal matrix. $\boldsymbol{H}_n$ can be first measured in the VLCP IoT network.

Here, given the AP selection and SG allocation, we aim to obtain the optimized modulation order variables $\boldsymbol{M}$ and power allocation variables $\boldsymbol{P}$. The partial Lagrange function of problem (14) is expressed as

$$\begin{aligned} &\Upsilon(\boldsymbol{\beta}, \boldsymbol{\omega}, \boldsymbol{\chi}, \boldsymbol{M}, \boldsymbol{P}) \\ &= \sum_{l\in\mathcal{L}}\sum_{k\in\mathcal{K}} \alpha_{k,l} R_k + \sum_{k\in\mathcal{K}} \beta_k\Big(R_k - R_k^{\min}\Big) \\ &\quad + \sum_{k\in\mathcal{K}} \omega_k\left(\mathrm{RSE}_k^{\max} - \sqrt{\mathrm{tr}\big(\mathbf{J}^{-1}\big(\Theta_k, \boldsymbol{P}_{\mathrm{po}}\big)\big)}\right) \\ &\quad + \sum_{l\in\mathcal{L}} \chi_l\left(P_{\max} - \sum_{k\in\mathcal{K}}\sum_{n\in\mathcal{N}_l} \rho_{k,n,l} P_{n,l}\right) \end{aligned} \tag{23}$$

where $\boldsymbol{\beta} = \{\beta_k, \forall k\}$, $\boldsymbol{\omega} = \{\omega_k, \forall k\}$, and $\boldsymbol{\chi} = \{\chi_l, \forall l\}$ are the dual Lagrange multiplier vectors or variables for the constraints in (11), (13), and "d" in (14). Then, the dual function of the Lagrange function (23) can be given by

$$J(\boldsymbol{\beta}, \boldsymbol{\omega}, \boldsymbol{\chi}) = \max_{\boldsymbol{M},\mathbf{P}} \{\Upsilon(\boldsymbol{\beta}, \boldsymbol{\omega}, \boldsymbol{\chi}, \boldsymbol{M}, \boldsymbol{P})\}. \tag{24}$$

In (24), when the dual function value is optimized, we can get the optimized modulation order $\boldsymbol{M}$ and power allocation variables $\boldsymbol{P}$. The dual problem to the original problem (14) can be written as

$$\begin{aligned} &\min_{\boldsymbol{\beta},\boldsymbol{\omega},\boldsymbol{\chi}} \{J(\boldsymbol{\beta}, \boldsymbol{\omega}, \boldsymbol{\chi})\} \\ &\text{s.t. } \boldsymbol{\beta} \geq \mathbf{0}, \boldsymbol{\omega} \geq \mathbf{0}, \boldsymbol{\chi} \geq \mathbf{0}. \end{aligned} \tag{25}$$

The value of $J(\boldsymbol{\beta}, \boldsymbol{\omega}, \boldsymbol{\chi})$ can be computed by using the Lagrange dual decomposition method. Notably, $J(\boldsymbol{\beta}, \boldsymbol{\omega}, \boldsymbol{\chi})$ is a concave function due to the pointwise infimum of a set of affine functions of the Lagrange multipliers. Hence, we can use the subgradient method to solve the optimization problem (14) [41]. Due to space limitations, see [33] and [41] for all the solutions processes.

Accordingly, we present the solution process for the AP selection, SG allocation, adaptive modulation, and power allocation in the integrated VLCP IoT networks, as shown in Algorithm 2.

Algorithm 2 RM Approach

Initialize: Set the iteration $j = 0$, set $R_{\mathrm{sum}}(0)$, $\boldsymbol{\alpha}(0)$, $\boldsymbol{\rho}(0)$, $\boldsymbol{M}(0)$, and $\boldsymbol{P}(0)$, the maximum tolerance $\varsigma > 0$;
1: **Repeat**
2: Update the AP selection variables $\boldsymbol{\alpha}(j+1)$ and the SG allocation variables $\boldsymbol{\rho}(j+1)$ by **Algorithm 1**;
3: Update the modulation order variables $\boldsymbol{M}$ and power allocation variables $\boldsymbol{P}(j+1)$ by solving (14) using the subgradient method with the partial Lagrange function in (23);
4: $j \leftarrow j + 1$;
5: Update the sum data rate $R_{\mathrm{sum}}(j)$;
6: Until $|R_{\mathrm{sum}}(j) - R_{\mathrm{sum}}(j-1)| \leq \varsigma$;
7: **End**
8: **Output**: $\boldsymbol{\alpha}(j)$, $\boldsymbol{\rho}(j)$, $\boldsymbol{M}(j)$ and $\boldsymbol{P}(j)$.

D. Complexity Analysis

The optimal AP selection and SG allocation can be achieved if we adopt the exhaustive search for all the possible SG allocation cases. In the multicell IoT network with the K-device, L cells and N SGs per cell, it is prohibitive to search the optimum due to the high computational complexity, since the exhaustive search method has $O(K^{N\times L})$ possible SG allocation cases. However, the complexity of our proposed suboptimal AP selection and SG allocation is $O(K \times N \times L)$, which is greatly lower than the exhaustive search method.

Let Z denote the number of the employed reference points (RPs) in the integrated VLCP network. The computational complexity of the applied RSS positioning approach is $O(L)$, while the computational complexity of the popular fingerprint positioning approach based on RSSI can be expressed as $O(LZ)$ [8]. Moreover, Bisio *et al.* [9], [10] compared and discussed some existing fingerprint positioning approaches, such as fingerprint positioning based on the Bayesian processes, Gaussian processes, and HORUS method. Let V denote the number of observation vectors of the Gaussian processes and let L' denote the number of APs necessary to converge to a location estimation. The computational complexity of the above-mentioned positioning approaches is summarized in Table II.

TABLE II
COMPLEXITY ANALYSIS OF POSITIONING APPROACHES

Approach	Complexity
RSS	$O(L)$
Low-complexity fingerprint [45]	$O(\log(L+Z))$
Fingerprint with dense RPs [48]	$O(L+Z)$
Fingerprint based on RSSI [8]	$O(LZ)$
Fingerprint based on Bayesian [10]	$O(4*\sum_{l=1}^{L'}(8.8l+6.2)*\|Z(l)\|)$
Fingerprint based on Gaussian [10]	$O(8.8LZ+15.9Z-1)$
Fingerprint based on HORUS [10]	$O(8.8LZ+9.1Z+(V+1)Z)$

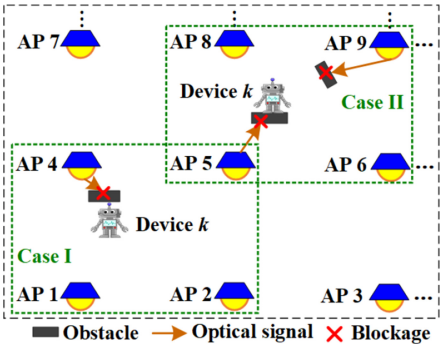

Fig. 3. Two cases of LOS blockages in integrated VLCP IoT networks.

A reduced fingerprint map is constructed in [45], containing only the data from the APs present in the query fingerprint. Reference fingerprints within the reduced map are used to localize the user. In [45], the complexity is reduced to $O(\log(L+Z))$ under the assumption that the number of RPs at which an AP is visible and the number of APs visible at an RP are both less than 20. This may not hold if the density of the fingerprint map is increased through interpolation or crowdsourcing. In that case, the complexity of the algorithm is in $O(L+Z)$ [46]. We would like to mention that some simple fingerprinting methods have low computational complexity, and some other methods employ offline data processing to help online fingerprinting methods to perform localization fast and smoothly.

From Table II, we can observe that the computational complexity of the fingerprinting positioning approaches is higher than that of the mentioned RSS positioning approach. However, it is worth noting that the fingerprinting positioning approaches can significantly improve the positioning accuracy compared with the RSS positioning approach (performance comparisons are shown in Section VI), but they require a lot of labeled data to train the localization model which needs extra computation and storage space at devices, which is not applicable for those IoT devices who require low computational complexity.

V. ROBUST OPTIMIZED SCHEMES UNDER BLOCKAGES

In practical indoor environments, the optical signals being broadcast from VLC APs to the devices may be blocked by obstacles due to the movement of devices or human beings, as shown in Fig. 3 (we take cases I and II as examples to analyze the negative effect of blocked links on the network performance). In this case, LOS is often blocked and none-LOS (NLOS) cannot support effective communication and positioning services, leading to the degradation of the network performance.

In details, in case I, for the kth device, the optical signal from its currently associated AP 4 is blocked by an obstacle, hence, the received SINR value is significantly reduced, resulting in decreasing the satisfied QoS levels and the network data rate. In this case, although the signal from AP 4 is blocked, the 2-D location of device k can be still successfully estimated by using the RSSI values from AP 1, AP 2, and AP 5, the device needs to select another AP to continue its service. However, in case II, the optimal signals being broadcasted from a number of APs (such as AP 5 and AP 9, even more APs) to the kth device are missing. In this case, it is hard to estimate the locations of devices with high positioning accuracy only using less than two RSSI values. Moreover, the data rate performance is degraded in this case as well.

According to the above analysis, how to estimate the locations of the devices with high positioning accuracy and how to guarantee the minimum data rate requirements of devices are still key challenges under blockages in the dynamic integrated VLCP IoT networks.

Hence, the following sections introduce two proposed schemes to address the above-mentioned challenges, in order to improve both the communication and positioning performance under LOS blockages.

A. Robust Handover Among APs

1) Handover Under Blockages: Due to the mobility of IoT devices, human beings, and obstacles, for any device, its current LOS link from the associated AP may be blocked in one time slot or even a long time duration. In this case, the device's performance and satisfied QoS level are notably affected. Hence, we propose a robust handover scheme to combat the LOS link blockage in the IoT network.

Once the device detects that its current LOS link is blocked, it reports the blockage information to the controller. The controller performs the handover mechanism based on the priority level of the device.

a) Handover for primary devices: If the device's location is fixed for a long period, the controller immediately selects the nearest AP to continually provide the communication services for the device. On the contrary, if the device is in the state of movement, the controller selects the device's neighboring AP based on the device's mobility trajectory where the device is moving toward the neighboring AP and the AP will be the nearest one for some time slots in the future. This handover mechanism aims to provide the stable and low-latency services for primary devices under blockages.

b) Handover for secondary devices: When the device detects the LOS blockage, the controller waits of a dwell period of τ_{wait}. When τ_{wait} expires, the controller selects one neighboring AP with the enough channel resource for the device; otherwise, the device still associates with its currently serving AP until the blocked link is recovered. This handover mechanism can effectively avoid

the potential ping-pong effects by reducing the unnecessary handovers.

2) Handover Under Mobility: Some literatures proposed the handover mechanisms based on the location information of devices [28]–[33], but they assumed that the devices' location information is perfectly known. Hence, we present a transmission handover mechanism based on the RSSI values.

Let $P_{k,l}^{\text{rec}}$ and $P_{k,\hat{l}}^{\text{rec}}$ denote the RSSI values of the kth device's currently serving AP and one candidate AP of its neighboring APs, respectively. The handover is executed when the following condition is satisfied:

$$P_{k,\hat{l}}^{\text{rec}} \geq P_{k,l}^{\text{rec}} + \varepsilon \quad \forall \hat{l} \in \mathcal{L} \tag{26}$$

where ε denotes the hysteresis value of the handover margin which is also used to prevent the unnecessary handovers. If the device locates in the region of the $\hat{l}$th AP and the RSSI value satisfied (26) for a certain period, then the device switches the connection from its currently serving AP l to the $\hat{l}$th AP.

B. Robust Positioning Scheme Under Blockages

As shown in Fig. 4(a), the kth device only receives the optical signals from AP 1 and AP 2 while the available signals being broadcasted from other APs are missing by obstacles. According to the RSSI signals received from AP 1 and AP 2, two circles centered at these two APs are identified with the black lines. The intersection of the two circles generates two possible locations [the black dots shown in Fig. 4(a)] of the kth device at the time slot t, denoted by $A^{(1)}(x_{k,t}^{(1)}, y_{k,t}^{(1)})$ and $A^{(2)}(x_{k,t}^{(2)}, y_{k,t}^{(2)})$, respectively. These two possible locations $A^{(1)}$ and $A^{(2)}$ can be calculated by solving the following two equations:

$$\begin{aligned}\sqrt{\left(x_1^{\text{led}} - x_{k,t}^{(1)}\right)^2 + \left(y_1^{\text{led}} - y_{k,t}^{(1)}\right)^2} &= d_{1,k,t} \\ \sqrt{\left(x_2^{\text{led}} - x_{k,t}\right)^2 + \left(y_2^{\text{led}} - y_{k,t}\right)^2} &= d_{2,k,t}\end{aligned} \tag{27}$$

where $d_{l,k,t}$ denotes the distance from the lth AP to device k at the time slot t which can be calculated by (8).

We would like to mention that [42] presented a simple scheme to select the most likely current location from these two possible locations, where the scheme calculates the distances from the previous location to the two possible locations and selects the possible location as the current location with the smallest distance. However, the scheme in [42] did not consider the movement behaviors of devices, hence, it still has the high positioning errors during devices' traveling under blockages.

In order to improve the positioning accuracy under blockages, we present a new robust positioning scheme by combining the PDR method [35] with the RSS-based VLP system (called PDR-assisted RSS), where PDR is the process of predicting the device' current location by using the previous locations' information.

In PDR, each device has its corresponding movement prediction model by sampling its periodical location information. When only one device receives at most two RSSI signals from the APs and other optical RSSI signals

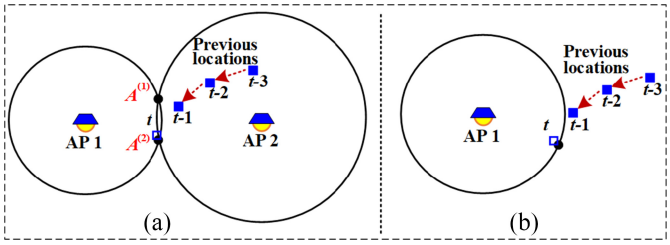

Fig. 4. (a) Signals only observed from AP 1 and AP 2 while the available signals from other APs are blocked. (b) Signal only observed from AP 1 while the available signals from other APs are blocked.

are missing at one time slot, it adopts PDR to calculate its velocity components $v_{k,x}$ and $v_{k,y}$ along the x-axes and y-axes from the previous location information $(x_{k,t-1}, y_{k,t-1})$ and $(x_{k,t-2}, y_{k,t-2})$ taken at the time slots $t-1$ and $t-2$. Here, the velocity components in the last time slot can be computed by

$$\begin{aligned}v_{k,t-1}^{x} &= \left(x_{k,t-1} - x_{k,t-2}\right)/\tau_{t-1} \\ v_{k,t-1}^{y} &= \left(y_{k,t-1} - y_{k,t-2}\right)/\tau_{t-1}\end{aligned} \tag{28}$$

respectively, and τ_{t-1} is the time duration at the time slot $t-1$.

After calculating the velocity components by (28) according to the two latest previous location samples, the kth device predicts its location at the current time slot t by performing the following formulas:

$$x'_{k,t} = x_{k,t-1} + v_{k,t-1}^{x}\tau_t; \quad y'_{k,t} = y_{k,t-1} + v_{k,t-1}^{y}\tau_t. \tag{29}$$

According to the above analysis, the kth device predicts its current location P' [the blue hollow square in Fig. 4(a)] by adopting the PDR method and calculates the possible locations ($A^{(1)}$ and $A^{(2)}$) by using the RSS positioning algorithm. In this case, the predicted location P' is close to one of the possible locations ($A^{(1)}$ and $A^{(2)}$) due to the movement behavior of devices, especially, in the indoor positioning environments. This allows the selection of the most likely current location of the device through comparing the distances between the predicted location and the two possible locations, i.e.,

$$\begin{aligned}d_{k,t}^{P'\to A^{(1)}} &= \sqrt{\left(x'_{k,t} - x_{k,t}^{(1)}\right)^2 + \left(y'_{k,t} - y_{k,t}^{(1)}\right)^2} \\ d_{k,t}^{P'\to A^{(2)}} &= \sqrt{\left(x'_{k,t} - x_{k,t}^{(2)}\right)^2 + \left(y'_{k,t} - y_{k,t}^{(2)}\right)^2}.\end{aligned} \tag{30}$$

The most likely current position $(x_{k,t}, y_{k,t})$ at the current time slot t is selected from the two possible locations by

$$\left(x_{k,t}, y_{k,t}\right) = \begin{cases} \left(x_{k,t}^{(1)}, y_{k,t}^{(1)}\right), & d_{k,t}^{P'\to A^{(1)}} \leq d_{k,t}^{P'\to A^{(2)}} \\ \left(x_{k,t}^{(2)}, y_{k,t}^{(2)}\right), & d_{k,t}^{P'\to A^{(1)}} > d_{k,t}^{P'\to A^{(2)}} \end{cases}. \tag{31}$$

If $d_{k,t}^{P'\to A^{(1)}} = d_{k,t}^{P'\to A^{(2)}}$, the kth device will choose the possible location with its current value $v_{k,t}^{x}/v_{k,t}^{y}$ being most likely with $v_{k,t-1}^{x}/v_{k,t-1}^{y}$ at the previous time slot, but the probability of $d_{k,t}^{P'\to A^{(1)}} = d_{k,t}^{P'\to A^{(2)}}$ is very small, which is negligible.

If the device receives only the RSSI signal from one AP while the other RSSI signals broadcast from APs are missing, as shown in Fig.4(b), according to the RSSI signal from

AP 1, one circle centered at AP 1 is identified and the possible location of the device is on the circle. By adopting the PDR method, the device predicts its current location P' [the blue hollow square in Fig. 4(b)], and the most likely current position of the device (the black dot) is selected on the circle with the minimum distance from it to the predicted location P'. It is worth noting that all RSSI signals being broadcasted from all APs to the device may be blocked in dynamic indoor environments, but it happens with a very small probability. In this case, the device can directly adopt the PDR positioning method to predict its current location according to the previous location samples.

VI. Simulation Results and Discussion

In this section, simulations are conducted in MATLAB 2017a to evaluate the performance of our presented integrated VLCP IoT network, the proposed RM approach and the robust schemes under LOS blockages.

We consider a typical indoor room with an area of 10 m $\times$ 10 m $\times$4 m, where 4 $\times$ 4 VLC APs are uniformly distributed at a height of 3.75 m. A number of devices are randomly distributed at two different heights (0.5 m and 1 m). $K/2$ devices need both communication and positioning services with low data rate (1 Mb/s per device) and other $K/2$ devices only require communication services with the high data rate requirement (10 Mb/s per device). The number of SGs in each cell is $N = 6$. For each AP, the LED lamp semi-angle at half power and the Lambertian emission order are 60° and 1, respectively. The active area, the FOV, the concentrator refractive index, and the responsivity of the PD are 1 cm^2, 110°, 1.5, and 0.5 A/W, respectively. The gain of the optical filter is 1. The dwell period of τ_{wait} is 1 s.

The transmission modulation bandwidth is 20 MHz and the available bandwidth is 10 MHz due to the Hermitian symmetry [4], [28], [36]. The range of the positioning frequencies is from 5.0 to 6.45 MHz. The modulation order $M = \{4, 8, 16, 32, 64, 128, 256, 512, 1024\}$ and $\text{BER}_{\max} = 3.8 \times 10^{-3}$. In addition, the positioning error threshold is 5 cm.

A. Performance Comparisons of Integrated VLCP Networks

Fig. 5(a) and (b) shows the positioning result and the cumulative distribution function (CDF) of the positioning errors over the indoor room, respectively. From Fig. 5(a), the mean positioning errors of our proposed approach, the existing approach [17], and the fingerprint-based indoor positioning approach are 4.28, 19.55, and 3.22 cm, respectively. Compared with the existing OFDMA-based integrated VLCP [17], our presented OFDM-SCM-interleaving integrated VLCP achieves the higher positioning accuracy. Among the three positioning approach, the fingerprint-based indoor positioning approach has the highest positioning accuracy, but it requires a lot of labeled data to train the localization model which is not suitable for those IoT devices as they require low computational complexity.

From Fig. 5(b), we can see that the positioning errors at 90% confidence for OFDM-SCM-interleaving-based integrated VLCP design, OFDMA-based integrated VLCP approach, and fingerprint-based indoor positioning approach are 6.37, 26.81, and 5.08 cm, respectively, showing a significant improvement of positioning accuracy by using the OFDM-SCM interleaving-based integrated VLCP approach and fingerprint-based indoor positioning approach. Even though the fingerprint-based indoor positioning approaches achieves higher positioning than the presented OFDM-SCM interleaving-based integrated VLCP approach, it needs extra computation and storage space at devices.

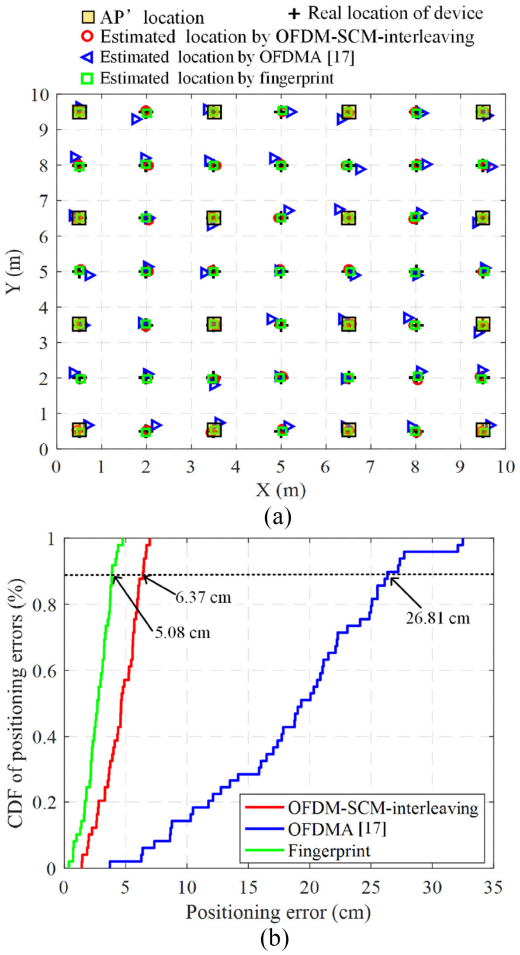

Fig. 5. Comparisons of (a) positioning results and (b) positioning errors' CDFs for the three different positioning approaches.

B. Performance Comparisons Versus Transmit Power Levels

In this section, we compare the performance of different RM approaches in our presented multicell integrated VLCP IoT network, where the approaches are shown as follows.

1) Optimal RM approach (denoted as optimal QoS-driven RM) uses the exhaustive search method to find the optimal AP selection and SG allocation strategy.
2) Our proposed suboptimal RM approach (denoted as proposed QoS-driven RM), with the purpose of guaranteeing the QoS requirements of the IoT devices while maximizing the overall data rate.
3) The load balancing (LB) approach without satisfying QoS support first [29] (denoted as LB RM [29]).

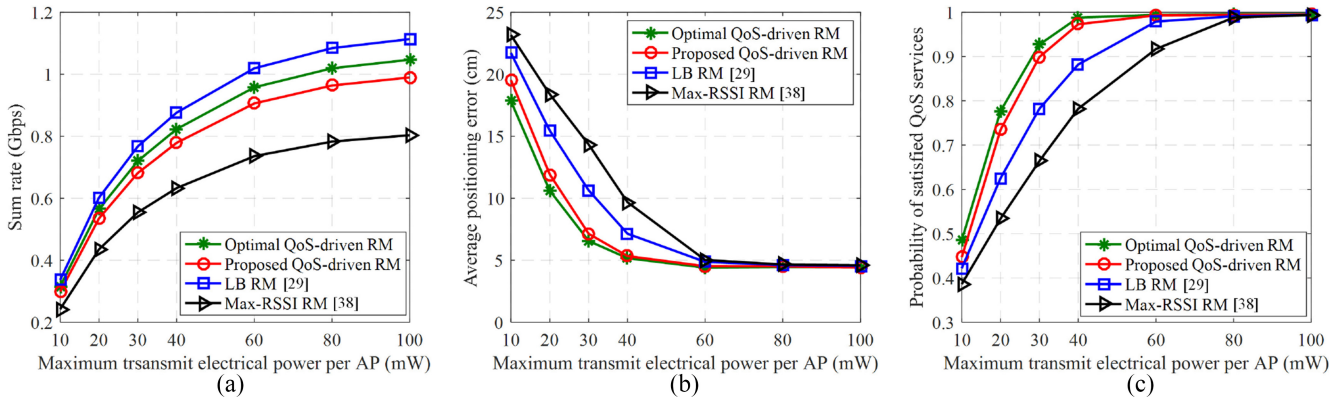

Fig. 6. Performance evaluations and comparisons versus the maximum transmit electrical power per AP.

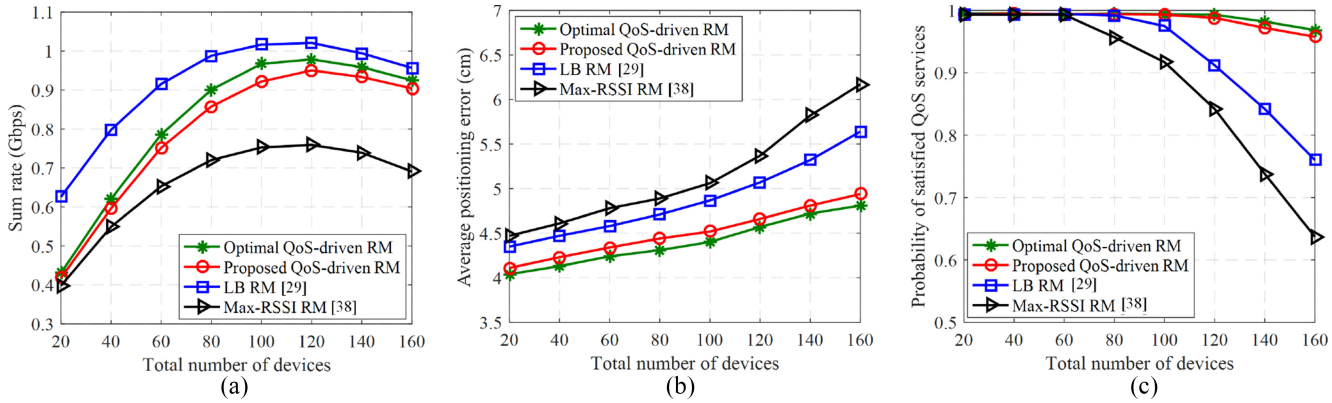

Fig. 7. Performance evaluations and comparisons varying total number of devices.

4) The RM approach-based the maximal RSSI [38] (denoted as max-RSSI RM [38]).

Fig. 6 shows the sum data rate of devices, the positioning error, and the probability of satisfied QoS services versus the electronic transmit power $P_{\max}$ per AP for the four approaches, when the total number of devices is $K = 100$ and the blocking probability of LOS link is 0.1. As the increase of $P_{\max}$, for all approaches, the sum data rate performance and the probability of satisfied QoS services increase, and the positioning error decreases. This is because that when $P_{\max}$ increases, the received SINR and received power allocated on the positioning subcarriers enhance, leading to the performance improvement. The data rate of the proposed RM approach achieves about 1.31 Gb/s when $P_{\max} = 100$ mW per AP.

From Fig. 6, although LB RM outperforms our proposed QoS-driven RM in terms of the data rate, it has the higher positioning error and the lower satisfied QoS level than the proposed QoS-driven RM. The max-RSSI RM approach archives the worst performance in the IoT networks because each device selfishly selects its own nearest AP, leading to the unbalanced resource allocation.

From Fig. 6(b), as $P_{\max}$ increases, the positioning error of all approaches decreases significantly when $P_{\max} < 60$ mW, but the performance is appropriately maintained at a horizontal level when $P_{\max}$ exceeds 60 mW. Such the performance improvement results from the high received power on positioning subcarriers when $P_{\max}$ is large. Once the positioning accuracy requirements are guaranteed in the high power region, the extra power will be allocated to maximize the sum rate of devices as shown in the optimization problem (14), thus the positioning accuracy performance is constant when $P_{\max}$ is in the high region. In addition, in Fig. 6(a), the improvement rate of the performance is not obvious when $P_{\max} >80$ mW, because ICI is one of the key factors which limits the data rate enhancement in the multicell IoT networks.

C. Performance Comparisons Under Various Device Density

Fig. 7 shows the performance comparisons of the four approaches versus the total different numbers of devices when $P_{\max} = 60$ mW and the blocking probability is 0.1. It can be seen that the data rate is constantly increasing to a peak due to the more probability of searching devices having good channel gains to enhance the sum rate. After that, it then declines as K increases further, because the increased number of handovers limits the data rate improvement and the more resource may need to allocate to the devices with poor channel gains to support their QoS requirements. Similarly, when the number of devices is large, all devices aim to share the limited power and bandwidth resource, hence, the positioning error slightly increases and the satisfied QoS level reduces.

In addition, we can observe that the proposed QoS-driven RM approach has comparable data rate performances to the

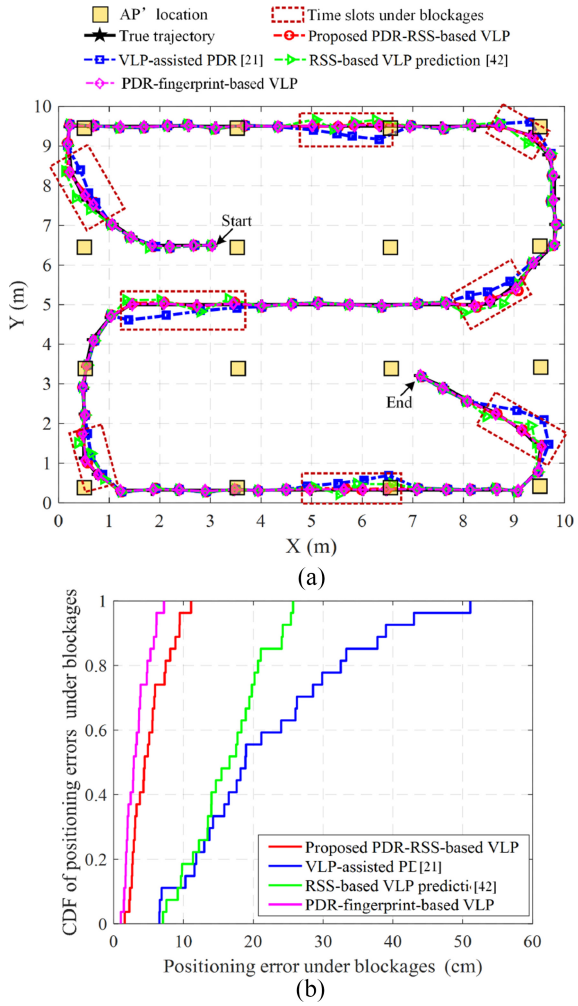

Fig. 8. (a) Trajectory performance comparisons of the three positioning schemes under blockages. (b) CDFs of positioning errors under blockages.

LB RM approach when the number of devices is large and outperforms the max-RSSI RM approach. Moreover, the proposed QoS-driven RM approach significantly achieves the higher satisfied QoS levels and the lower positioning error than both the LB RM and max-RSSI RM approaches for the large number of devices. The proposed QoS-driven RM approach achieves a satisfied QoS level improvement of up to 20.3% compared with LB RM (non-QoS-driven RM) approach

Because the proposed approach aims to search the QoS-driven optimized strategy to effectively meet the different QoS requirements of devices while maintaining the high data rate performance, thereby improving the device experiences in the indoor IoT networks.

D. Performance Comparisons Under Blockages

This section compares the performance of the proposed and existing approaches. For the positioning schemes, we compare the indoor tracking performance of the following positioning schemes under blockages.

1) Our proposed robust positioning scheme by combining PDR with the RSS-based VLP (denoted as PDR-RSS-based VLP).
2) The VLP-assisted PDR positioning scheme, similar to [21] (denoted as VLP-assisted PDR [21]).
3) The RSS-based VLP positioning scheme by using the previous location information to predict devices' locations under blockages [42] (denoted as RSS-based VLP prediction [42]).
4) Combining PDR with the fingerprint-based VLP (denoted as PDR-fingerprint-based VLP).

The indoor tracking performances over a 2-D indoor floor for the three positioning schemes under blockages are provided in Fig. 8(a). All the four schemes have the similar positioning accuracy performance under the LOS condition (no blockages). However, the positioning error is large for the VLP-assisted PDR scheme [21] under blockages, and it is further increased as the traveling distance increases in this case. Because the positioning error will gradually increase over time using the PDR method to predict devices' locations under blockages. By contrast, the best positioning performance is achieved by using our proposed PDR-RSS-based VLP, where the information of the RSS results are used to correct the positioning error under blockages, hence, the trajectory is pulled back to the true path as analyzed in Section V-B. In addition, the RSS-based VLP with prediction scheme [42] obtains the high positioning error under blockages because it does not consider the movement behaviors of devices and choose the most likely predicted location based on the previous information, hence, it still has the high positioning errors during devices' traveling in this case.

The CDFs of the positioning errors of the three schemes under blockages are shown in Fig. 8(b). The mean positioning errors of the PDR-RSS-based VLP, VLP-assisted PDR, RSS-based VLP prediction, and PDR-fingerprint-based VLP schemes under LOS blockage events are 5.13, 21.97, 16.35, and 4.02 cm, respectively.

Fig. 9 shows the robustness of the three positioning schemes against the LOS blockages. When the blocking probability increases, the positioning error obviously increases for the VLP-assisted PDR and RSS-based VLP prediction schemes while it slightly increases for the PDR-RSS-based VLP scheme. Moreover, the gap of the performances between them becomes larger with the increased value of the blocking probability. The above positioning results indicate the effectiveness of the proposed robust scheme against the LOS blockages in the IoT networks.

The effect of the blocking probability of LOS links on the sum data rate and the satisfied QoS level are shown in Fig. 10. From Fig. 10(a), the data rate performances of all approaches are decreased upon increasing the LoS blocking probability. However, our proposed approach with robust handover can still achieve a good performance and it outperforms the LB RM approach when the blocking probability is more than 0.3. In addition, the probability of the satisfied QoS services decreases during this process because the blockage significantly degrades the received desired power or SINR, results in failing to guarantee the different QoS requirements of devices. However, for all blocking probabilities, our proposed approach still outperforms other approaches.

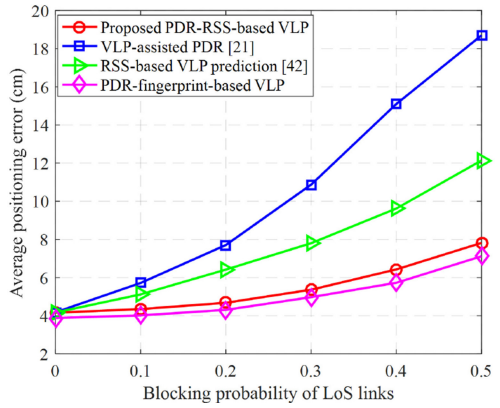

Fig. 9. Average positioning error comparisons against the blocking probability of LOS links.

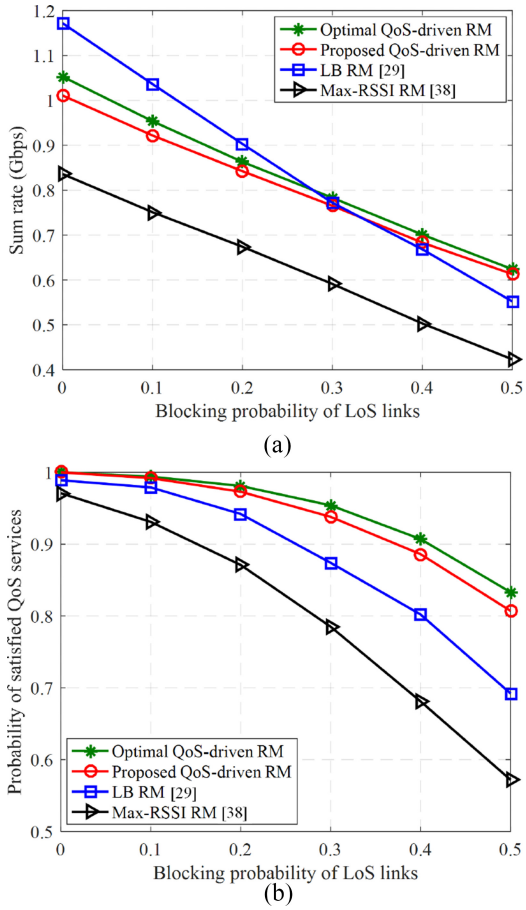

Fig. 10. Performance evaluations and comparisons against the blocking probability of LOS links.

VII. Extended Applications of the Presented Work for IoT

The presented integrated VLCP is capable of supporting high-speed data transmission and content-intensive Internet applications (e.g., photographs, messages, control information, videos audio, videos transmission, and live streaming) for the massive number of IoT devices in smart city, smart industry, smart health, and smart building. The IoT networks can utilize VLC medium to communicate between the IoT devices and the associated cloud (Internet) with high-speed capacity, resulting in fast data transmission and less data stored on the cloud as well as the low transmission latency. In addition, it is worth noting that big smart complexes, shopping marts, airports, factories, hospitals, smart car parks, underwater communications, and transportation entities need such presented integrated VLCP architecture to support real-time applications securely at high-speed and high-accuracy tracking.

1) Indoor Localization and Tracking: In the indoor IoT networks, there still lacks an indoor localization solution that can answer the needs of various location-based IoT applications with desired simplicity, robustness, accuracy, and responsiveness [20]–[25], [43]. VLC-based localization has the ability to achieve the real-time localization with high localization accuracy compared with RF-based positioning systems, which makes it suitable for real-time tracking of IoT devices [20]–[25], [43]. VLP for IoT environments can be used for indoor positioning of forklifts, tracking of indoor robots or indoor vehicles, and aerial drones to carry out autonomous tasks. For example, unmanned aerial vehicles (UAVs), also known as drones, offer a safe and cost-effective way for hard-to-reach areas for tasks such as visual inspections [20]–[25], [43].

2) Energy Harvesting: In the indoor IoT environments, there exist some energy-constrained devices, e.g., sensors for monitoring, humidity and indoor air quality, etc. Hence, it is important to extend the lifetime of the devices due to their limited energy budget. In our presented VLCP network, at each IoT device, light energy harvesting is achieved by using PD and the harvested energy is used for collected data reporting through the RF uplink [14], [15]. Hence, the presented integrated VLCP network-based light energy harvesting can provide the potentials to charge the IoT devices in indoor scenarios.

3) Provide Security and Safety for IoT: Our presented integrated VLCP network provides inherent security, since visible light signals do not penetrate walls [1]–[3]. Such a secrecy feature is an important requirement for IoT applications such as the ones for Industry 4.0. In addition, visible light signals do not generate the electromagnetic interference so it can be applied in the electromagnetic interference-sensitive IoT environments (e.g., hospitals, airports, and gas stations).

4) Underwater IoT Communication: Underwater communication is important for underwater observation and sea monitoring. However, in underwater environments, conventional RF-based systems do not effectively work due to the high attenuation of RF signals, and acoustic (sonar) wave cannot provide high data rate even though it has low attenuation. By contract, visible light is capable of supporting the high data rate over short distances in underwater, and this could enable divers and underwater vehicles effectively communicate with each other [44].

VIII. Conclusion

In this article, we presented a new integrated VLCP IoT network to support the high-speed data transmission and high-accuracy positioning services for indoor IoT devices.

In order to satisfy different QoS requirements (ranging from the minimum data rate and high positioning accuracy), a QoS-driven optimized joint AP selection, SG allocation, adaptive modulation, and power allocation approach was proposed in the integrated VLCP IoT network. After that, a low-complexity iterative algorithm was presented to solve the RM optimization problem. Furthermore, the robust handover mechanism and PDR-assisted VLCP scheme were presented to maintain good network performance under blockages. The simulation results verified the superiority in the performance of the presented integrated VLCP IoT network and also showed that the proposed approach and robust schemes outperform other existing solutions in terms of improving the data rate and guaranteeing devices' QoS requirements. VLC-only networks face some challenges, such as lack of uplink support, susceptibility to LOS blocking, and small coverage area, but these challenges can be addressed by combining RF with VLC. Hence, the co-deployment of RF and VLC networks is a straightforward way to overcome the above-mentioned shortcomings and highlight its advantages [1]–[3].

REFERENCES

[1] N. Saxena, A. Roy, B. J. R. Sahu, and H. Kim, "Efficient IoT gateway over 5G wireless: A new design with prototype and implementation results," *IEEE Commun. Mag.*, vol. 55, no. 2, pp. 97–105, Feb. 2017.

[2] B. Khalfi, B. Hamdaoui, and M. Guizani, "Extracting and exploiting inherent sparsity for efficient IoT support in 5G: Challenges and potential solutions," *IEEE Wireless Commun.*, vol. 24, no. 5, pp. 68–73, Oct. 2017.

[3] D. Karunatilaka, F. Zafar, V. Kalavally, and R. Parthiban, "LED based indoor visible light communications: State of the art," *IEEE Commun. Surveys Tuts.*, vol. 17, no. 3, pp. 1649–1678, 3rd Quart., 2015.

[4] H. Haas, L. Yin, Y. Wang, and C. Chen, "What is LiFi?," *J. Lightw. Technol.*, vol. 34, no. 6, pp. 1533–1544, Mar. 15, 2016.

[5] L. Wan, G. Han, L. Shu, S. Chan, and N. Feng, "PD source diagnosis and localization in industrial high-voltage insulation system via multimodal joint sparse representation," *IEEE Trans. Ind. Electron.*, vol. 63, no. 4, pp. 2506–2516, Apr. 2016.

[6] C. Röhrig and M. Müller, "Indoor location tracking in non-line-of-sight environments using a IEEE 802.15.4a wireless network," in *Proc. IEEE/RSJ Int. Conf. Intell. Robots Syst.*, 2009, pp. 552–557.

[7] M. F. Keskin, A. D. Sezer, and S. Gezici, "Localization via visible light systems," *Proc. IEEE*, vol. 106, no. 6, pp. 1063–1088, Jun. 2018.

[8] S. He and S.-H. G. Chan, "Wi-Fi fingerprint-based indoor positioning: Recent advances and comparisons," *IEEE Commun. Surveys Tuts.*, vol. 18, no. 1, pp. 466–490, 1st Quart., 2016.

[9] I. Bisio, F. Lavagetto, M. Marchese, and A. Sciarrone, "Performance comparison of a probabilistic fingerprint-based indoor positioning system over different smartphones," in *Proc. Int. Symp. Perform. Comput. Telcommun.*, Toronto, ON, Canada, 2013, pp. 161–166.

[10] I. Bisio, F. Lavagetto, M. Marchese, and A. Sciarrone, "Smart probabilistic fingerprinting for WiFi-based indoor positioning with mobile devices," *Pervasive Mobile Comput.*, vol. 31, pp. 107–123, Feb. 2016.

[11] "Cisco service provider Wi-Fi: A platform for business innovation and revenue generation," San Jose, CA, USA, Cisco, White Paper, Nov. 2012.

[12] L. I. Albraheem, L. H. Alhudaithy, A. A. Aljaser, M. R. Aldhafian, and G. M. Bahliwah, "Toward designing a Li-Fi-based hierarchical IoT architecture," *IEEE Access*, vol. 6, pp. 40811–40825, 2018.

[13] X. Liu, X. Wei, L. Guo, Y. Liu, Q. Song, and A. Jamalipour, "Turning the signal interference into benefits: Towards indoor self-powered visible light communication for IoT devices in industrial radio-hostile environments," *IEEE Access*, vol. 7, pp. 24978–24989, 2019.

[14] S. Shao, A. Khreishah, and H. Elgala, "Pixelated VLC-backscattering for self-charging indoor IoT devices," *IEEE Photon. Technol. Lett.*, vol. 29, no. 2, pp. 177–180, Jan. 15, 2017.

[15] G. Pan, H. Lei, Z. Ding, and Q. Ni, "3-D hybrid VLC-RF indoor IoT systems with light energy harvesting," *IEEE Trans. Green Commun. Netw.*, vol. 3, no. 3, pp. 853–865, Sep. 2019.

[16] Y. Wang, X. Wu, and H. Haas, "Distributed load balancing for Internet of Things by using Li-Fi and RF hybrid network," in *Proc. IEEE 26th Annu. Int. Symp. Pers. Indoor Mobile Radio Commun. (PIMRC)*, Hong Kong, 2015, pp. 1289–1294.

[17] Y. Xu *et al.*, "Accuracy analysis and improvement of visible light positioning based on VLC system using orthogonal frequency division multiple access," *Opt. Exp.*, vol. 26, no. 7, pp. 9230–9242, Apr. 2018.

[18] B. Lin, X. Tang, Z. Ghassemlooy, C. Lin, and Y. Li, "Experimental demonstration of an indoor VLC positioning system based on OFDMA," *IEEE Photon. J.*, vol. 9, no. 2, pp. 1–9, Apr. 2017.

[19] H. Yang, P. Du, W. Zhong, C. Chen, A. Alphones, and S. Zhang, "Reinforcement learning based intelligent resource allocation for integrated VLCP systems," *IEEE Wireless Commun. Lett.*, vol. 8, no. 4, pp. 1204–1207, Aug. 2019.

[20] X. G. Liu, X. Wei, and L. Guo, "DIMLOC: Enabling high-precision visible light localization under dimmable LEDs in smart buildings," *IEEE Internet Things J.*, vol. 6, no. 2, pp. 3912–3924, Apr. 2019.

[21] Y. Wang and H. Zhao, "Improved smartphone-based indoor pedestrian dead reckoning assisted by visible light positioning," *IEEE Sensors J.*, vol. 19, no. 8, pp. 2902–2908, Apr. 2019.

[22] P. Du, S. Zhang, C. Chen, A. Alphones, and W.-D. Zhong, "Demonstration of a low-complexity indoor visible light positioning system using an enhanced TDOA scheme," *IEEE Photon. J.*, vol. 10, no. 4, pp. 1–10, Aug. 2018.

[23] S. Shao, A. Khreishah, and I. Khalil, "Enabling real-time indoor tracking of IoT devices through visible light retroreflection," *IEEE Trans. Mobile Comput.*, to be published, doi: 10.1109/TMC.2019.2901665.

[24] Y. Zhuang, Q. Wang, M. Shi, P. Cao, L. Qi, and J. Yang, "Low-power centimeter-level localization for indoor mobile robots based on ensemble Kalman smoother using received signal strength," *IEEE Internet Things J.*, vol. 6, no. 4, pp. 6513–6522, Aug. 2019.

[25] S. Ma, Q. Liu, and P. C.-Y. Sheu, "Foglight: Visible light-enabled indoor localization system for low-power IoT devices," *IEEE Internet Things J.*, vol. 5, no. 1, pp. 175–185, Feb. 2018.

[26] H. Yang, C. Chen, W.-D. Zhong, A. Alphones, S. Zhang, and P. Du, "Demonstration of a quasi-gapless integrated visible light communication and positioning system," *IEEE Photon. Technol. Lett.*, vol. 30, no. 23, pp. 2001–2004, Dec. 2018.

[27] M. Obeed, A. M. Salhab, S. A. Zummo, and M.-S. Alouini, "New algorithms for energy-efficient VLC networks with user-centric cell formation," *IEEE Trans. Green Commun. Netw.*, vol. 3, no. 1, pp. 108–121, Mar. 2019.

[28] M. A. Dastgheib, H. Beyranvand, J. A. Salehi, and M. Maier, "Mobility-aware resource allocation in VLC networks using T-step look-ahead policy," *J. Lightw. Technol.*, vol. 36, no. 23, pp. 5358–5370, Dec. 1, 2018.

[29] X. Li, F. Jin, R. Zhang, J. Wang, Z. Xu, and L. Hanzo, "Users first: User-centric cluster formation for interference-mitigation in visible-light networks," *IEEE Trans. Wireless Commun.*, vol. 15, no. 1, pp. 39–53, Jan. 2016.

[30] H. Yang, C. Chen, W.-D. Zhong, and A. Alphones, "Joint precoder and equalizer design for multi-user multi-cell MIMO VLC systems," *IEEE Trans. Veh. Technol.*, vol. 67, no. 12, pp. 11354–11364, Dec. 2018.

[31] R. Jiang, Q. Wang, H. Haas, and Z. Wang, "Joint user association and power allocation for cell-free visible light communication networks," *IEEE J. Sel. Areas Commun.*, vol. 36, no. 1, pp. 136–148, Jan. 2018.

[32] C. Chen, W.-D. Zhong, H. Yang, S. Zhang, and P. F. Du, "Reduction of SINR fluctuation in indoor multi-cell VLC systems using optimized angle diversity receiver," *J. Lightw. Technol.*, vol. 36, no. 17, pp. 3603–3610, Sep. 1, 2018.

[33] H. Yang, C. Chen, and W.-D. Zhong, "Cognitive multi-cell visible light communication with hybrid underlay/overlay resource allocation," *IEEE Photon. Technol. Lett.*, vol. 30, no. 12, pp. 1135–1138, Jun. 15, 2018.

[34] B. G. Guzmán, A. A. Dowhuszko, V. P. G. Jiménez, and A. I. Pérez-Neira, "Robust cooperative multicarrier transmission scheme for optical wireless cellular networks," *IEEE Photon. Technol. Lett.*, vol. 30, no. 2, pp. 197–200, Jan. 15, 2018.

[35] A. R. Jimenez, F. Seco, C. Prieto, and J. Guevara, "A comparison of pedestrian dead-reckoning algorithms using a low-cost MEMS IMU," in *Proc. IEEE WISP*, Budapest, Hungary, 2009, pp. 37–42.

[36] R. Mesleh, H. Elgala, and H. Haas, "On the performance of different OFDM based optical wireless communication systems," *IEEE/OSA J. Opt. Commun. Netw.*, vol. 3, no. 8, pp. 620–628, Aug. 2011.

[37] M. F. Keskin and S. Gezici, "Comparative theoretical analysis of distance estimation in visible light positioning systems," *J. Lightw. Technol.*, vol. 34, no. 3, pp. 854–865, Feb. 1, 2016.

[38] Q. Ye, B. Rong, Y. Chen, M. Al-Shalash, C. Caramanis, and J. G. Andrews, "User association for load balancing in heterogeneous cellular networks," *IEEE Trans. Wireless Commun.*, vol. 12, no. 6, pp. 2706–2716, Jun. 2013.
[39] T. Bu, L. Li, and R. Ramjee, "Generalized proportional fair scheduling in third generation wireless data networks," in *Proc. IEEE INFOCOM*, Apr. 2006, pp. 1–12.
[40] Y. Wang, L. Tao, Y. Wang, and N. Chi, "High speed WDM VLC system based on multi-band CAP64 with weighted pre-equalization and modified CMMA based post-equalization," *IEEE Commun. Lett.*, vol. 18, no. 10, pp. 1719–1722, Oct. 2014.
[41] S. Boyd and L. Vandenberghe, *Convex Optimization*. Cambridge, U.K.: Cambridge Univ. Press, 2004.
[42] T. T. Son, H. Le-Minh, F. Mousa, Z. Ghassemlooy, and N. V. Tuan, "Adaptive correction model for indoor MIMO VLC using positioning technique with node knowledge," in *Proc. IEEE ComManTel*, 2015, pp. 94–98.
[43] Y. Almadani, M. Ijaz, S. Rajbhandari, U. Raza, and B. Adebisi, "Dead-zones limitation in visible light positioning systems for unmanned aerial vehicles," in *Proc. IEEE Int. Conf. Ubiquitous Future Netw. (ICUFN)*, Zagreb, Croatia, 2019, pp. 419–421.
[44] M. Elamassie, F. Miramirkhani, and M. Uysal, "Performance characterization of underwater visible light communication," *IEEE Trans. Commun.*, vol. 67, no. 1, pp. 543–552, Jan. 2019.
[45] S. M. J. Sadegh, S. Shahidi, and S. Valaee, "An efficient database management for cloud-based indoor positioning using Wi-Fi fingerprinting," in *Proc. IEEE 26th Annu. Int. Symp. Pers. Indoor Mobile Radio Commun. (PIMRC)*, Oct. 2017, pp. 1–6.
[46] S. A. Razavi, M. Valkama, and E. S. Lohan, "K-means fingerprint clustering for low-complexity floor estimation in indoor mobile localization," in *Proc. IEEE Globecom Workshops (GC Wkshps)*, Dec. 2015, pp. 1–7.

Helin Yang (S'15) is currently pursuing the Ph.D. degree with the School of Electrical and Electronic Engineering, Nanyang Technological University, Singapore.

He serves as a reviewer for IEEE international journals, such as the *IEEE Communications Magazine*, the IEEE TRANSACTIONS ON WIRELESS COMMUNICATIONS, and the IEEE TRANSACTIONS ON VEHICULAR TECHNOLOGY. His current research interests include wireless communication, visible light communication, Internet of Things, and resource management.

Wen-De Zhong (SM'03) received the B.S. degree from the Beijing University of Posts and Telecommunications, Beijing, China, in 1982, and the M.Eng. and Ph.D. degrees from the University of Electro Communications, Tokyo, Japan, in 1990 and 1993, respectively.

He was a Post-Doctoral Fellow with the NTT Network Service and System Laboratories, Tokyo, from 1993 to 1995. He was a Senior Research Fellow with the Department of Electrical and Electronic Engineering, University of Melbourne, Melbourne, VIC, Australia, from 1995 to 2000. In 2000, he joined Nanyang Technological University, Singapore, as an Associate Professor, where he became a Full Professor in 2009, and is currently with the School of Electrical and Electronic Engineering. His current research interests include visible light communication/positioning, optical fiber communication systems and networks, optical access networks, and signal processing.

Chen Chen (S'13–M'19) received the B.S. and M.Eng. degrees from the University of Electronic Science and Technology of China, Chengdu, China, in 2010 and 2013, respectively, and the Ph.D. degree from Nanyang Technological University, Singapore, in 2017.

He is currently a Tenured-Track Assistant Professor with the School of Microelectronics and Communication Engineering, Chongqing University, Chongqing, China. His research interests include visible light communications, Li-Fi, visible light positioning, optical access networks, and digital signal processing.

Arokiaswami Alphones (M'92–SM'98) received the B.Tech. degree from Madras Institute of Technology, Chennai, India, in 1982, the M.Tech. degree from the Indian Institute of Technology Kharagpur, Kharagpur, India, in 1984, and the Ph.D. degree in optically controlled millimeter wave circuits from Kyoto Institute of Technology, Kyoto, Japan, in 1992.

Since 2001, he has been with the School of Electrical and Electronic Engineering, Nanyang Technological University, Singapore. His current research interests include electromagnetic analysis on planar RF circuits and integrated optics, microwave photonics, metamaterial-based leaky wave antennas, and wireless power transfer technologies.

Pengfei Du received the B.Eng. degree in mechanical engineering from Sichuan University, Chengdu, China, in 2011, and the Ph.D. degree in optical engineering from Tsinghua University, Beijing, China, in 2016.

From 2016 to 2019, he was a Research Fellow with Nanyang Technological University, Singapore. Since 2019, he has been a Scientist with the A*STAR's Singapore Institute of Manufacturing Technology, Singapore. His current research interests include industrial IoT, lidar, visible light positioning, Li-Fi, optical IoT, and quantum detection.